Raman study of the phonon symmetries in BiFeO₃ single crystals

C. Beekman,[1,*] A. A. Reijnders,[1] Y. S. Oh,[2] S. W. Cheong,[2] and K. S. Burch[1]

[1]*Department of Physics and Institute of Optical Sciences, University of Toronto, 60 St. George Street, Toronto, Ontario, Canada M5S 1A7*

[2]*Rutgers Center for Emergent Materials and Department of Physics and Astronomy, Rutgers University,*
136 Frelinghuysen Road, Piscataway, New Jersey 08854, USA

In bismuth ferrite (BiFeO₃), antiferromagnetic and ferroelectric order coexist at room temperature, making it of particular interest for studying magnetoelectric coupling. The mutual control of magnetic and electric properties is very useful for a wide variety of applications. This has led to an enormous amount of research into the properties of BiFeO₃. Nonetheless, one of the most fundamental aspects of this material, namely the symmetries of the lattice vibrations, remains controversial. We present a comprehensive Raman study of BiFeO₃ single crystals with the approach of monitoring the Raman spectra while rotating the polarization direction of the excitation laser. Our method results in unambiguous assignment of the phonon symmetries and explains the origin of the controversy in the literature. Furthermore, it provides access to the Raman tensor elements enabling direct comparison with theoretical calculations. Hence, this allows the study of symmetry breaking and coupling mechanisms in a wide range of complex materials and may lead to a noninvasive, all-optical method to determine the orientation and magnitude of the ferroelectric polarization.

PACS number(s): 78.30.−j, 72.10.Di, 75.85.+t

Multiferroic BiFeO₃ (BFO) is one of the few materials that simultaneously exhibits a robust magnetic ordering and large spontaneous ferroelectric polarization at room temperature,[1] making it of particular interest for studying magnetoelectric coupling.[2–4] The mutual control of magnetic and electric properties is of great interest for applications in spintronics and magnetic storage media.[5] This has triggered significant interest in BFO, resulting in numerous studies including optical[6,7] and Raman spectroscopy,[8–10] theoretical calculations,[11,12] thin-film devices,[1,13] and electrical control of magnetic excitations.[14–18] Among these various techniques, the Raman spectrum of BFO is one of the most widely studied as it is a powerful tool to investigate phonons, magnons, and their interaction (i.e., electromagnons).[16–19] Moreover, proper phonon mode assignment is necessary to describe the phonons critical for the multiferroic behavior. However, even for measurements taken along the high-symmetry directions of single crystals, controversy in the symmetry assignments of the phonon modes remains. The discrepancies have previously been ascribed to violation of Raman selection rules due to variations in strain fields[9] (i.e., multidomain states) caused by polishing of the crystal surface. Once the symmetries are unambiguously assigned, deviations in phonon mode behaviors could be used to detect the presence of symmetry breaking, multidomain states, and phonon-magnon interactions. Furthermore, simply determining the mode symmetry only allows for a qualitative comparison with theoretical calculations, whereas a quantitative comparison is enabled by measuring the Raman tensor elements.

To this end we have performed a comprehensive set of polarized micro-Raman spectroscopic studies of BFO single crystals with uniform ferroelectric polarization. Careful examination and proper modeling of the rotational dependence of the Raman intensity enables us to unambiguously assign the (A_1, E_x, and E_y) modes. Furthermore, we use the presented model to show that slight misalignment of the crystal leads to ambiguity in the symmetry assignments. Indeed, our

data reveal that comparison of spectra obtained for different scattering geometries at a single polarization vector of the incoming light is not sufficient to have truly unambiguous mode assignment. Nonetheless, unambiguous assignment can be reached on the as-grown single crystal when the Raman mode intensities as a function of crystal rotation are measured (consistent with previous work on sapphire[20]). Hence, with the presented method polishing is omitted and the resulting ambiguity from misalignment can be avoided.

The as-grown BFO single crystals used in this work have pseudocubic $(100)_{pc}$ facets with a ferroelectric single-domain state[21] (see Supplemental Material[22]). The crystal structure of BFO (rhombohedral distorted perovskite, $R3c$) shows a transition from high to low symmetry accompanied by the formation of spontaneous electric polarization below the transition temperature $T_C \sim 1100$ K.[23] The ferroelectricity is ascribed to lattice distortions (i.e., off-centering of the Bi ions) and results from softening and subsequent freezing of the lowest frequency polar-phonon mode. The antiferromagnetic ordering sets in below $T_N \sim 640$ K with a large magnetic moment of 4 μ_B on the Fe ions. Canting of the spins leads to a cycloidal spin structure with large period (62 nm)[23,24] rotating in the plane containing the electric polarization vector **P** and cycloid wave vector q. At room temperature BFO has a perovskite pseudocubic unit cell ($a \sim 3.96$ Å) elongated along the $(111)_{pc}$ direction coinciding with **P**. The point group is C_{3v}, with 13 Raman active modes, of which four have A_1 symmetry (i.e., propagate along the c-axis) and nine have either E_x or E_y symmetry (i.e., propagate in the x-y plane), which are doubly degenerate. When the laser is not along the c-axis, phonons can propagate in the x-z plane, which could lead to LO-TO splitting (i.e., lifts the degeneracy) and hence the presence of A(TO) modes in the XX and E(LO) modes in the XY geometry,[25–27] which further complicates the analysis.

The Raman spectra were taken in a backscattering configuration with a Horiba Jobin Yvon LabRam microscope with a 532 nm excitation source and a 10× objective (0.8 NA),
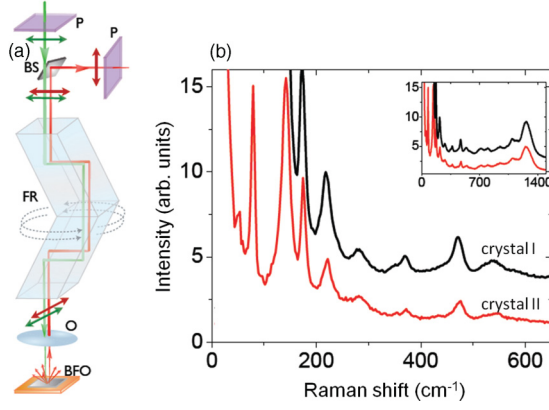
FIG. 1. (Color online) (a) Experimental setup with the Fresnel rhomb (FR) used to rotate the polarization of the incoming laser. The green beam is the excitation laser and the red the Raman scattered light, with polarizers (P), notch filter (BS), objective (O) to focus down the laser and the sample (BFO). (b) Typical single-phonon spectra in XX geometry for two different $[100]_{pc}$ crystals (black: crystal I and red: crystal II) for Raman shifts between 0 and 650 cm^{-1}. Inset: Full range up to 1500 cm^{-1}. The curves are vertically translated for clarity.

TABLE I. Phonon mode frequencies, the Raman tensor elements (a, b, d, e, and f) for the modes as obtained from the fits, and the symmetry assignments for crystal I. The data for all the modes are presented in the Supplemental Material (Ref. 22).

mode	a	b	d	e	f	symm.
140	–	–	155.0	–38.4	–12.6	Ey(TO)
173	–	–	125.1	42.4	10.8	Ey(TO)
220	–	–	80.1	–25.5	–5.7	Ey(TO)
265	visible on (111)pc and (100)pc (XY only)					A(LO)
279	very weak					?
288	–	–	60.2	–56.5	–14.9	Ey(TO)
350	–56.3	86.4	–	–	–	A(LO)
371	–	–	–20.8	16.2	42.2	Ex(TO)
471	–	–	–32.7	19.3	65.1	Ex(TO)
520	–49.7	77.3	–	–	–	A(LO)
550	–	–	36.8	–18.7	–2.3	Ey(TO)

resulting in a collection area of $\sim$1 μm (see Supplemental Material[22]). All data presented in this work are taken at room temperature. Furthermore, we investigate the polarization dependence of the Raman spectra by linearly polarizing the excitation laser in the plane of the sample and rotating the polarization direction with steps of $10°$ over a total of $180°$. The rotation is accomplished via a $\lambda/2$ Fresnel rhomb and is fully equivalent to an in-plane rotation of the sample [see Fig. 1(a) and Supplemental Material[22]]. A second polarizer is used to analyze the scattered light, which is either parallel (XX) or perpendicular (XY) to the incoming polarization direction.

Figure 1(b) shows typical Raman spectra (XX scattering geometry) taken on two different crystals [both with a $(100)_{pc}$ surface]. The modes below 600 cm^{-1} are single-phonon modes and the broad features above 600 cm^{-1} [see inset Fig. 1(b)] are ascribed to 2-phonon excitations, which is in agreement with previous reports.[9] The spectrum taken on crystal I shows a total of 11 single-phonon modes (see Table I), while crystal II shows a total of 13 single-phonon modes (i.e., all modes observed in crystal I and two additional modes at 53 and 77 cm^{-1}, which can be seen due to the use of a better filter with a lower cutoff frequency). Raman intensities taken on different locations on one crystal and on different crystals [Fig. 1(b)] show similar polarization dependencies (i.e., the symmetry assignments are consistent), which confirms the single-domain character of the crystals. By comparing the polarization dependence of the Raman intensities of crystal I and II we show how a different (but homogeneous) ferroelectric polarization direction influences the phonon mode behaviors (discussed in detail below). In Fig. 2 we show the evolution of the Raman spectra as a function of in-plane crystal rotation (i.e., rotation of the polarization direction) taken on the $(100)_{pc}$ surface of crystal I for the XX [Fig. 2(a)] and XY [Fig. 2(b)] scattering geometries. Furthermore, we normalize the Raman spectra at 1500 cm^{-1} to correct for any power fluctuations of the laser and for polarization dependence of the reflectivity of the crystal. We have also confirmed that

the anisotropy of the optical constants[28] does not significantly influence polarization dependence of the Raman spectra (see Supplemental Material[22]). To quantitatively analyze the data the spectra are fitted with multiple Lorentzian oscillators of the form $I(\omega) = I_0 + \sum_i (\frac{A_i \Gamma_i}{[4(\omega - E_i)^2 + \Gamma_i^2]})$, where i is the peak number, I_0 accounts for the background, E_i is the center frequency, Γ_i is the width, and A_i is the area of peak i. The fitting is done with fixed mode positions, extracting mode peak intensity $[I_i(E_i)]$ from the ratio between area and width of the fitted oscillators [i.e., $I_i(E_i) = A_i / \Gamma_i$].
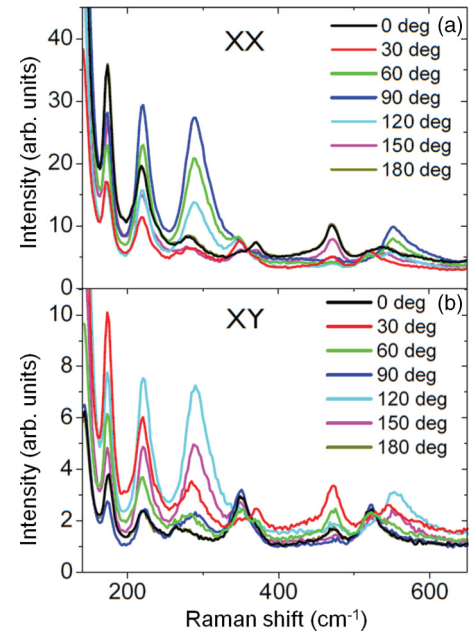

FIG. 2. (Color online) The evolution of Raman spectra as the Fresnel rhomb is rotated. (a) XX scattering geometry. (b) XY scattering geometry. The spectra were taken on the as-grown $[100]_{pc}$ surface of crystal I.
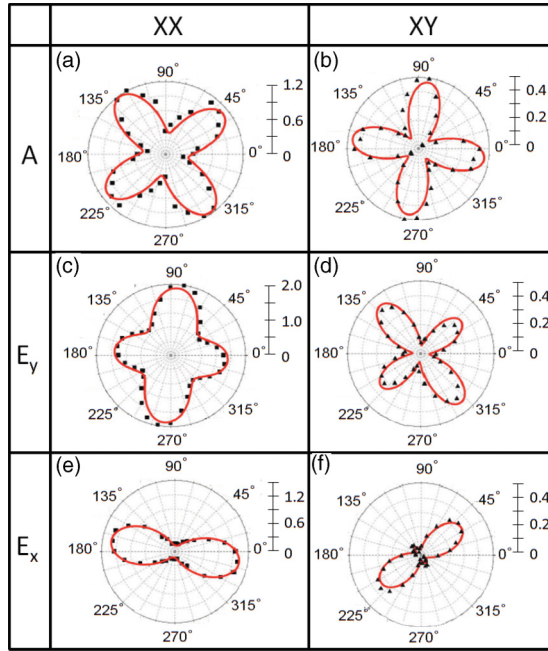
FIG. 3. (Color online) Polar plots of the mode intensities determined from the Raman spectra (left: *XX* and right: *XY*) as function of polarization rotation for three representative modes [(a) and (b), mode at 350 cm^{-1}; (c) and (d), mode at 140 cm^{-1}; and (e) and (f), mode at 471 cm^{-1}] measured on crystal I. The solid lines are fits (350 cm^{-1}: A, 140 cm^{-1}: E_y, and 471 cm^{-1}: E_x) of which the tensor elements are indicated in Table I.

In Fig. 3 we show the mode intensities as determined from fitting the Raman spectra as a function of polarization angle for three representative modes. The polar plots indicate the presence of exactly three different mode symmetries. Not surprisingly we have found that all modes can be sorted into one of these three types. Indeed, the fits in Fig. 3 show that these three types match well with what we expect for the A, E_x, and E_y symmetries. Here we note that the differences between the mode behaviors can be subtle; for example the *XY* curves for the A and the E_y modes [see Figs. 3(b) and 3(d)] look similar. Hence, simultaneous modeling of the full polarization curves for both *XX* and *XY* is necessary and only then results in unambiguous assignment of the modes.

Moreover, we find no evidence that we are probing phonons that propagate in the x-z plane (i.e., oblique phonons[26,27]). Indeed, such modes would exhibit LO-TO splitting as seen previously, with the presence of A(TO) and E(LO) modes leading to reduced intensities of the A(LO) and E(TO) modes.[27] Hence, we observe the 13 modes expected from group theory and the modeling shows that the phonons transform according to the zone center modes' irreducible representations. Furthermore, on a polished c-axis surface we find the same number of modes as for the as-grown surface with the modes at the same frequencies (within our resolution).

With a closer look at the model we used for the fits in Fig. 3 we can explain why there is controversy in the phonon mode assignment in the literature. The extracted mode intensities as a function of polarization angle are modeled using the Raman tensors for the C_{3v} point group (i.e., the trigonal symmetry of the lattice). The Raman intensity as a function of polarization

angle can be calculated using the equation[20,29]

$$I = |e_s^\dagger R^\dagger \alpha R e_i|^2, \qquad (1)$$

in which α are the C_{3v} Raman tensors in a trigonal basis,[30]

$$A = \begin{pmatrix} a & 0 & 0 \\ 0 & a & 0 \\ 0 & 0 & b \end{pmatrix} E_x = \begin{pmatrix} 0 & d & 0 \\ d & 0 & e \\ 0 & f & 0 \end{pmatrix} E_y = \begin{pmatrix} d & 0 & -e \\ 0 & -d & 0 \\ -f & 0 & 0 \end{pmatrix},$$

$$(2)$$

with R the matrix that rotates from cubic to the trigonal orientation, and with e_s and e_i the polarization vectors that describe the scattered and incoming light, respectively. The polar plots for the calculated Raman mode intensity as a function of polarization rotation are shown in Figs. 4(a)–4(c). Here we have assumed that the Poynting vector is perfectly parallel to the c-axis [111] of the crystal resulting in easy to distinguish behaviors of the modes. Indeed, in this case determination of A modes should be easy [Fig. 4(a)]; their intensity is independent of the polarization angle and should have no measurable intensity in the *XY* geometry. However, at certain angles of crystal orientation [indicated by dotted lines in Figs. 4(b) and 4(c)] one can still mistake an E mode for an A mode (i.e., the mode has intensity in the *XX* geometry but disappears in the *XY* geometry). Additional error can come from slight misalignment of the c-axis with respect to the propagation of the Raman laser light (i.e., surface normal). Figures 4(d)–4(f) demonstrate that for the A, E_x, and E_y modes, respectively, introduction of a few degrees misalignment can lead to large variations in the intensity of
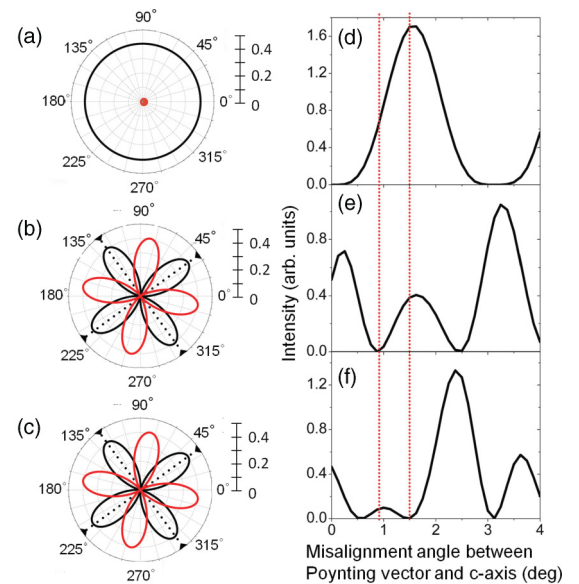

FIG. 4. (Color online) (a)–(c) Polar plots of calculated mode intensity variations as function of polarization angle for A, E_y, and E_x symmetry, respectively, in the case of the perfect alignment of the Poynting vector with c-axis (black: *XX*, red: *XY*). The dotted lines in (b) and (c) indicate angles for which E modes will be mistakenly assigned as A modes. (d)–(f) Linear plots of the calculated intensity variations in the A, E_x, and E_y modes, respectively (for *XY* scattering geometry) as function of the deviation of the c-axis from the surface normal. The dotted lines indicate misalignment angles (0.9° and 1.5°) for which the symmetry of 2 out of 3 modes will be misassigned.

the phonon modes (in the *XY* geometry), and hence crossover in mode symmetry assignments. The two dotted lines in Figs. 4(d)–4(f) are examples of misalignment angles (0.9° and 1.5°, respectively) for which the symmetry of 2 out of 3 modes will be misassigned. Also, the Raman beam is typically focused down, resulting in an average of incident angles, which already introduces some misalignment. Here we note that our method results in the same mode symmetry assignments compared to Palai *et al.*,[9] measured on a polished *c*-axis surface. However, we also show that the standard method of just monitoring the disappearance of modes when switching from *XX* to *XY* scattering geometry does not provide adequate information to unambiguously assign the phonon mode symmetries. Our results not only unambiguously determine the mode symmetries but also explain the controversy in the literature and lead to direct determination of the Raman tensor elements.

In Table I we show the observed phonon mode frequencies, Raman tensor elements (*a*, *b*, *d*, *e*, and *f*) as obtained from the fits, and their symmetry assignments for the $[100]_{pc}$ surface of crystal I. We provide the corresponding polarization curves in the Supplemental Material.[22] Moreover, on crystal II, 13 modes were observed (i.e., the correct amount according to group theory) at the same frequencies and with the same assignments as presented in Table I; two additional modes were observed at 53 and 77 cm^{-1}; the tensor elements and symmetry assignments for all modes observed on crystal II are shown in Table T1 in the Supplemental Material.[22] Here we note that the symmetry assignment of the mode at 279 cm^{-1} remains challenging, because it is very weak and shouldering the very strong E_y mode at 288 cm^{-1}. We have also checked the Raman spectra on a polished $[111]_{pc}$ (i.e., *c*-axis) surface (data not shown) on which we observed a total of 13 modes (the mode at 53 cm^{-1} disappeared while an additional mode appeared at 70 cm^{-1}). The mode at 70 cm^{-1} remains unassigned; it probably also exists on the $[100]_{pc}$ surface but is too weak and close to a strong *E* mode to be clearly visible. Furthermore, it is possible that the mode at 53 cm^{-1} is indicative of a violation of Raman selection rules due to symmetry breaking. Modes at this Raman shift have been previously assigned as *A*(TO) modes;[9] however, they should not be visible in our scattering geometry and we do not see evidence of the other *A*(TO) modes in our spectra. Alternatively this mode may be an electromagnon.[17] Future low-temperature studies, where the linewidths are narrow, would help to better assign these modes. Nonetheless, using the presented method we have unambiguously assigned the phonon modes and extracted the Raman tensor elements providing quantitative information for direct comparison with theoretical predications. Furthermore, the ratios between the Raman tensor elements *a* and *b* are identical for the *A* modes observed on both crystals. However, we do observe some differences between the ratios of the *E*-mode tensor elements between the measurements taken on crystals I and II, which in no way influences the

consistency of the symmetry assignments. These differences may indicate that the two crystals (both are single domain) have a different direction and/or magnitude of the ferroelectric polarization. This would indeed affect the *E* modes but not the *A* modes, since the *A* modes are fully symmetrical and constitute vibrations along the *c*-axis (i.e., parallel to the ferroelectric polarization direction). However, this could mean that changes in the ferroelectric polarization direction leave the mode symmetries unaltered. Hence, one needs the method presented here to observe this subtle effect (i.e., changes in the tensor element ratios of the *E* modes) of different ferroelectric polarization on the Raman intensities.

We have measured the evolution of polarized Raman spectra of BFO single crystals and extracted the polarization curves for every single-phonon mode for both the *XX* and the *XY* scattering geometry. We fitted the *XX* and *XY* curves simultaneously for each mode using a model based on the Raman tensors of the C_{3v} point group [Eq. (1)]. As a result unambiguous symmetry assignment and determination of Raman tensor elements of the phonon modes is accomplished even on the as-grown $[100]_{pc}$ surface. In Fig. 3 the excellent and unambiguous agreement between the experimental results and our calculations for a $[100]_{pc}$ surface demonstrates the importance of performing the Raman measurements over a full rotation of the crystal, whereas the calculations in Fig. 4 demonstrate that only measuring the *XX* and *XY* spectra on a $[111]_{pc}$ surface for a single polarization direction (as is typically done) can easily lead to wrong assignments of the phonons due to misalignment of the crystal. It is clear that unambiguous mode assignment can only be reached if one monitors the Raman signal as a function of rotation of the crystal. Simply comparing *XX* and *XY* scattering geometries for one polarization angle is not enough even for a *c*-axis surface. Besides obtaining unambiguous mode assignment for BFO, this work has wider implications as well. The method can be used on any material to check crystal symmetry and assign the phonon modes. Furthermore, once unambiguous assignment has been accomplished one can use the presented method to investigate symmetry breaking as well, for example by studying deviations in the tensor element ratios and the symmetry assignments and through observation of more than the predicted number of modes. This gives us a powerful tool to investigate occurrence of (electro)magnons and compare to existing reports.[17,18] Moreover it would allow study of coupling mechanisms in complex materials such as multiferroics, as well as provide quantitative information for direct comparison with theoretical predications.

---

*beekmanc@ornl.gov

[1] R. Ramesh and N. A. Spaldin, Nat. Mater. **6**, 21 (2007).

[2] T. Kimura *et al.*, Nature (London) **426**, 55 (2003).

[3] N. A. Hill, J. Phys. Chem. B **104**, 6694 (2000).

[4] P. Rovillain, R. de Sousa, Y. Gallais, A. Sacuto, M. A. Masson, D. Colson, A. Forget, M. Bibes, A. Barthlmy, and M. Cazayous, Nat. Mater. **9**, 975 (2010).

[5]W. Eerenstein, N. D. Mathur, and J. F. Scott, Nature (London) **442**, 759 (2006).

[6]R. P. S. M. Lobo, R. L. Moreira, D. Lebeugle, and D. Colson, Phys. Rev. B **76**, 172105 (2007).

[7]X. S. Xu, T. V. Brinzari, S. Lee, Y. H. Chu, L. W. Martin, A. Kumar, S. McGill, R. C. Rai, R. Ramesh, V. Gopalan, S. W. Cheong, and J. L. Musfeldt, Phys. Rev. B **79**, 134425 (2009).

[8]M. K. Singh, H. M. Jang, S. Ryu, and M.-H. Jo, Appl. Phys. Lett. **88**, 042907 (2006).

[9]R. Palai, H. Schmid, J. F. Scott, and R. S. Katiyar, Phys. Rev. B **81**, 064110 (2010) and references therein.

[10]A. A. Porporati, K. Tsuji, M. Valant, A.-K. Axelsson, and G. Pezzotti, J. Raman Spectrosc. **41**, 84 (2010).

[11]P. Hermet, M. Goffinet, J. Kreisel, and Ph. Ghosez, Phys. Rev. B **75**, 220102(R) (2007).

[12]J. B. Neaton, C. Ederer, U. V. Waghmare, N. A. Spaldin, and K. M. Rabe, Phys. Rev. B **71**, 014113 (2005).

[13]J. Wang, J. B. Neaton, H. Zheng, V. Nagarajan, S. B. Ogale, B. Liu, D. Viehland, V. Vaithyanathan, D. G. Schlom, U. V. Waghmare, N. A. Spaldin, K. M. Rabe, M. Wuttig, and R. Ramesh, Science **299**, 1719 (2003).

[14]S. Lee, W. Ratcliff, S.-W. Cheong, and V. Kiryukhin, Appl. Phys. Lett. **92**, 192906 (2008).

[15]D. Lebeugle, D. Colson, A. Forget, M. Viret, A. M. Bataille, and A. Goukasov, Phys. Rev. Lett. **100**, 227602 (2008).

[16]F. Wang, J.-M. Liu, and Z. F. Ren, Adv. Phys. **58**, 321 (2009).

[17]M. Cazayous, Y. Gallais, A. Sacuto, R. de Sousa, D. Lebeugle, and D. Colson, Phys. Rev. Lett. **101**, 037601 (2008).

[18]P. Rovillain, M. Cazayous, Y. Gallais, A. Sacuto, R. P. S. M. Lobo, D. Lebeugle, and D. Colson, Phys. Rev. B **79**, 180411(R) (2009).

[19]L. J. Sandilands, J. X. Shen, G. M. Chugunov, S. Y. F. Zhao, Shimpei Ono, Yoichi Ando, and K. S. Burch, Phys. Rev. B **82**, 064503 (2010).

[20]M. C. Munisso, W. Zhu, and G. Pezzotti, Phys. Status Solidi B **246**, 1893 (2009).

[21]T. Choi, S. Lee, Y. J. Choi, V. Kiryukhin, and S.-W. Cheong, Science **324**, 63 (2009); S. Lee, T. Choi, W. Ratcliff, R. Erwin, S-W. Cheong, and V. Kiryukhin, Phys. Rev. B **78**, 100101(R) (2008).

[22]See Supplemental Material at http://link.aps.org/supplemental/10.1103/PhysRevB.86.020403 for additional data and the table containing the Raman tensor elements and symmetry assignments for the phonons observed on crystal II.

[23]G. Catalan and J. F. Scott, Adv. Mater. **21**, 2463 (2009).

[24]M. Ramazanoglu, W. Ratcliff, Y. J. Choi, S. Lee, S.-W. Cheong, and V. Kiryukhin, Phys. Rev. B **83**, 174434 (2011) and references therein.

[25]R. Loudon, Adv. Phys. **13**, 423 (1964).

[26]J. Hlinka, J. Pokorny, S. Karimi, and I. M. Reaney, Phys. Rev. B **83**, 020101(R) (2011).

[27]G. Stone and V. Dierolf, Opt. Lett. **37**, 1032 (2012).

[28]S. G. Choi, H. T. Yi, S.-W. Cheong, J. N. Hilfiker, R. France, and A. G. Norman, Phys. Rev. B **83**, 100101 (2011).

[29]R. L. Moreira, M. R. B. Andreeta, A. C. Hernandes, and A. Dias, Crystal Growth and Design **5**, 1458 (2005).

[30]W. Hayes and R. Loudon, *Scattering of Light by Crystals* (John Wiley, New York, 1978).